



# Fretting Behavior of WC-Co-Cr Coatings Against QT Steel in Bolted Joint

Vilma Haaja<sup>1</sup> · Tommi Varis<sup>1</sup> · Jussi Laurila<sup>1</sup> · Matti Isakov<sup>1</sup>

Submitted: 31 August 2023 / in revised form: 16 January 2024 / Accepted: 22 January 2024  
© The Author(s) 2024

**Abstract** Fretting damage on contacting surfaces introduces major challenges in mechanical assemblies. Thermal sprayed hardmetal coatings are extensively used for surface modification in tribological applications under demanding conditions and may also be subjected to fretting-inducing loading. In the present work, the fretting behavior of High Velocity Oxy-Fuel (HVOF) and High Velocity Air-Fuel (HVOF) sprayed WC-10Co-4Cr coatings against quenched and tempered (QT) steel was studied by using a single bolt joint-type fretting experiment. This experimental approach was selected to obtain realistic data on the fretting fatigue performance of the contact pairs (both coating-to-steel and coating-to-coating). Experimental results were completed with continuum-scale linear elastic finite element method (FEM) calculations.

**Keywords** finite-element method · fretting fatigue · fretting wear · thermally sprayed coating · WC-10Co-4Cr

## Introduction

Thermally sprayed hardmetal coatings provide an effective means to improve the surface properties, such as wear and corrosion resistance, of load carrying components and structures in demanding loading conditions (Ref 1). Due to their excellent properties against different wear mechanisms under tribological conditions (Ref 2), they are used

in many applications subject to wear such as rollers in paper machines (Ref 3, 4), landing gears (Ref 5, 6), hydraulic cylinders (Ref 7, 8), pumps and valves (Ref 9), hydro turbines (Ref 10), and many other wear parts (Ref 11). In addition to these, the use of thermally sprayed hardmetal coatings also in fretting-inducing conditions has become an interesting research topic. Fretting is a commonplace phenomenon in various load carrying interfaces between components, such as in bolted joints, which are subjected to cyclic loading (Ref 12). Fretting is caused by micrometer-scale reciprocating movement between contact surfaces under frictional load, which leads to wear and fatigue crack nucleation on the contact surfaces, thus reducing service life (Ref 13, 14). Since fretting damage occurs between the contact surfaces inside the joint, the early detection of the damage is challenging, which may thus result in an unexpected and sometimes catastrophic failure of the component. Therefore, it is of great importance that both experimental and theoretical research are carried out to accurately predict fretting-induced surface damage and fatigue in engineering materials including thermally sprayed hardmetal coatings.

Due to the significance of fretting damage, several mitigation methods and palliatives have been studied over the years. Apart from design changes and the use of lubricants, several surface modification methods and coating techniques have been proposed as mitigation methods (Ref 15, 16). Certain coatings can be used as fretting palliatives; the effective mechanisms, however, are versatile and case-specific ranging from self-lubricating or strain-accommodating soft coatings to very hard coatings and to coatings with high residual compressive stress (Ref 15, 16). There is also a wide range of other reasons to use coatings in load carrying structures, such as for protection against aggressive environment or wear (Ref 17).

---

✉ Matti Isakov  
matti.isakov@tuni.fi

<sup>1</sup> Faculty of Engineering and Natural Sciences, Materials Science and Environmental Engineering, Tampere University, P.O.B 589, 33014 Tampere, Finland

Therefore, a given coating might inadvertently be subjected to fretting-inducing loading, the effects of which are often unknown for coated components. Given the risks and challenges related to fretting-induced damage, the behavior of the used coatings should be understood sufficiently also in this respect. In the case of hardmetal coatings, previous works in the literature have focused on the wear (Ref 3-10, 18-24), fatigue (Ref 5, 25-29) as well as fretting behavior (Ref 30-36). However, as argued in the following and demonstrated by the results of the current study, in terms of fretting-induced fatigue failure of hardmetal coated high-strength steels, the current body of knowledge does not seem to be sufficient.

Kubiak et al. Ref 33 studied the fretting resistance of WC-Co coatings against 30NiCrMo steel in sphere-to-plane contact. They found that the wear resistance and fretting fatigue strength are increased significantly by the application of shot peening treatment and hardmetal coating compared to plain steel. The addition of the coating was also observed to decrease the coefficient of friction (COF) between the contact surfaces. Based on their study Kubiak et al. Ref 33 concluded that the fretting fatigue limit corresponds to a fatigue crack arrest condition in the uncoated steel and to a nucleation threshold in the case of the coating. Similar results were obtained by Okane et al. Ref 34, who reported that WC-Co coating improves the fretting fatigue strength of a high-strength steel by delaying the onset of crack nucleation and slowing down crack propagation. Furthermore, the tangential forces at the contact were observed to be reduced by the coating especially at the early stages of cyclic loading and show a gradual increase alongside with increasing surface damage. Recently, Wang et al. Ref 35 studied fretting wear and fatigue mechanisms of WC-Co hardmetal coatings in contact with high-strength steel. They concluded that the main wear mechanism for the coating is abrasive wear and that the wear pits act as initiation sites for the fatigue cracks, but the abrasive wear might also increase fretting fatigue life by removing stress concentrations on the contact. Based on these studies, it thus appears that the hardmetal coating might improve the fretting fatigue performance of the substrate. It should be noted, however, that in the above-mentioned studies bulk cyclic loading was introduced only on the coated side of the contact, and the counterpart surface (pad, sphere) served only to introduce the fretting damage. It is therefore not fully clear how the introduction of a hardmetal coating on one or both of the surfaces affects the overall fretting fatigue behavior of the joint. This aspect will be one of the focus areas of the current study.

An additional challenge in studying the fretting properties of thermally sprayed hardmetal coatings is that their mechanical properties can be very different depending on

the method used to produce them. For example, comparing the properties of High Velocity Oxy-Fuel (HVOF) and High Velocity Air-Fuel (HVAF) coatings, typically HVAF coatings have better mechanical properties such as hardness, elastic modulus, and fracture toughness (Ref 22-24). They also tend to have lower porosity than HVOF coatings (Ref 23). These differences, which are related to the lower flame temperature and higher particle velocities of the HVAF process compared to the HVOF process, also seem to lead to a better wear resistance of the coatings (Ref 22-24). In particular, there are differences in the stress states of the coatings between the HVAF and HVOF processes. A WC-CoCr coating prepared by HVOF spraying almost always develops a relatively high tensile stress state, whereas the stress state developed in a HVAF coating can vary from a mild tensile stress state to a high compressive stress state (Ref 22). It has been shown that, particularly against cavitation erosion, where coating wear requires material removal through fatigue crack growth, a high compressive stress state slows crack growth and reduces coating wear (Ref 22). The residual stress state of a coating can also be expected to play a role in its fretting fatigue resistance.

The objective of the current study is to analyze the effects of hardmetal coating on the fretting-induced wear and fatigue in a realistic mechanical joint. For this, WC-10Co-4Cr High Velocity Oxy-Fuel (HVOF) and High Velocity Air-Fuel (HVAF) thermal sprayed hardmetal coatings were deposited on a high-strength quenched and tempered (QT) steel. Both coatings were prepared by spraying and subsequent mechanical grinding to a thickness of 250  $\mu\text{m}$  and to the same surface roughness as the steel counterpart (Ra 0.2  $\mu\text{m}$ ). These values were selected to represent typical applications. Furthermore, the HVAF coating was also prepared as a thin 90  $\mu\text{m}$  layer and tested in the as-sprayed condition. The purpose of this test series was to test the idea of a straightforward-to-apply protection on the interface. The contact pairs were studied by using the single bolt joint experimental arrangement developed by Juoksukangas et al. Ref 12. In this arrangement, the two contacting test pieces are subjected to the same bulk cyclic loading, which facilitates comprehensive analysis of the fretting fatigue behavior of the joint. Furthermore, the use of the bolt joint to generate the necessary contact conditions for fretting reduces the possible effects of imperfections at the specimen edges and increases the effective contact area, which is beneficial in the testing of coatings both in terms of specimen preparation and representativeness of the results. The use of large contact area is further supported by a recent report from Hintikka et al. Ref 37, who demonstrated that adhesion spots, which are a key mechanism in fretting damage, can in certain cases grow larger (over 1 mm) than the contact area in typical fretting

experiments. In order to obtain detailed data on the surface damage mechanisms as well as fatigue crack nucleation and propagation, a series of interrupted tests was carried out in the current study followed by an extensive microstructural characterization. The analysis was supplemented by continuum-scale linear elastic finite element method (FEM) calculations, which were used to predict the contact stresses and slip as well as the damage and crack initiation locations by means of frictional work and maximum stresses at the interface. The results of this study show that the effects of the hardmetal coating on the total fretting performance of the joint are dependent on the properties and behavior of the counterpart material.

## Materials and Methods

### Fretting Test Device

The fretting tests were carried out by using an in-house developed flat-on-flat fretting test device in so-called bolt joint configuration (Fig. 1). The test methodology was originally developed by Juoksukangas et al. Ref 12 for steel-to-steel contact and was modified in the current study for coating-to-steel and coating-to-coating contacts. As shown in Fig. 1, the test arrangement consists of two flat test specimens which are held together by a single strain gauge instrumented M8 bolt (with constant preload applied with torque prior to the test and controlled continuously, as explained below) and at one end by the main clamping. The specimens are subjected to bulk cyclic bending loading via eccentric mechanism connected to the opposite end (referred to as the “free end” throughout this paper). Fretting conditions at the contact interface between the specimens are created by the combination of the imposed bulk bending and the preload of the bolt; cyclic slip at the interface takes place because the contacting surfaces have always opposite signs of bending strain, whereas cyclic shear stresses at the interface result from the interfacial friction and the contact pressure created by the bolt preload. It should be noted that the bolt itself is not carrying any shear load due to the clearance between the bolt and the hole. Furthermore, the test arrangement does not allow for direct measurement of the contact stresses and slip. Instead, as discussed later, FEM calculations are used to determine the distribution of stresses and slip as well as the frictional dissipation at the contact interface. In short, the most severe fretting damage is expected to take place near the axial centerline on the free end side of the bolt hole.

During the experiments, data are collected from several sources: bolt preload (with strain gauges attached axially to the bolt), specimen bending displacement (with laser sensor) and specimen bending strain with four strain gauges

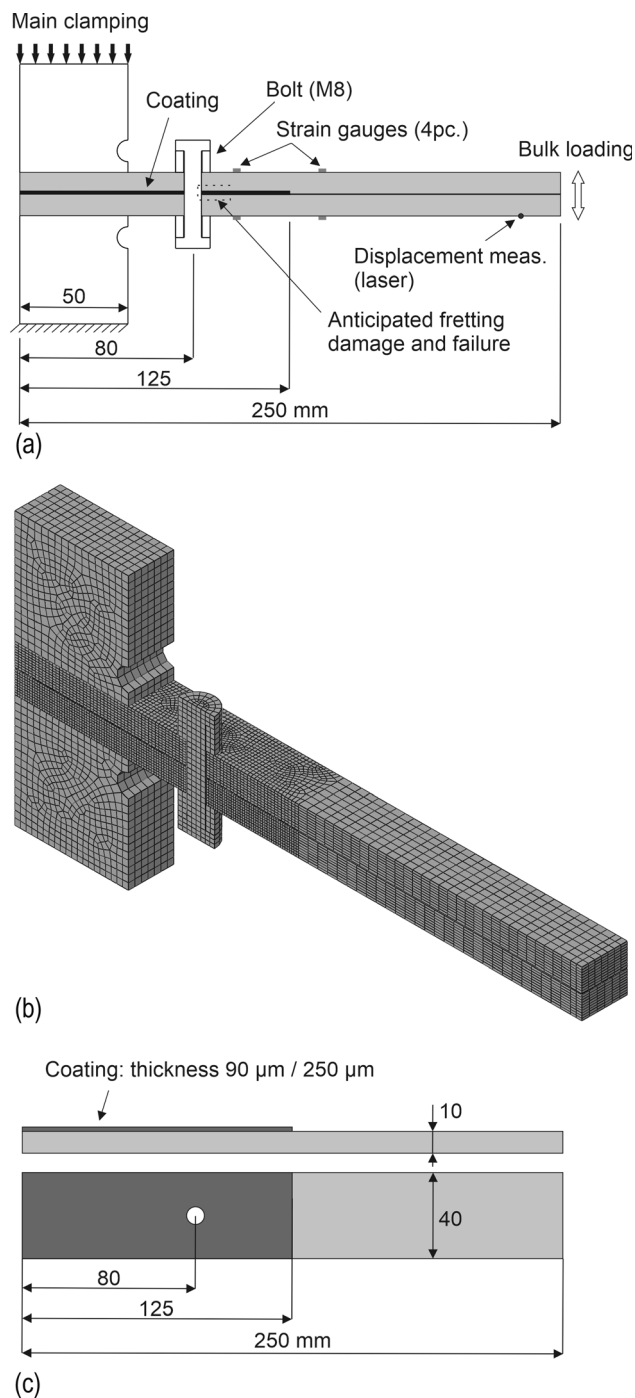


**Fig. 1** Illustration of (a) the fretting test setup and (b) the FEM model mesh (only half of the test setup is modeled due to symmetry) and (c) schematic depiction of the coated specimens

(two gauges on each specimen, as illustrated in Fig. 1a). As in Ref 12, the data from the strain gauges are linearly interpolated to obtain the nominal bulk stress at the center of the bolt hole.

## Materials and Test Specimens

A quenched and tempered steel EN 34CrNiMo6 obtained from Ovako Metals Oy Ab was used both for the substrate material of the coated specimens and for the plain steel specimens. The chemical composition and mechanical properties of the steel are shown in Tables 1 and 2, respectively. WC-Co-Cr powders WOKA 3652 and WOKA 3654 from Oerlikon Metco were used as feedstock materials for the coatings. Chemical composition and particle sizes of the powders are presented in Table 3. Both the steel substrates and the plain steel specimens were machined to a size of 250 mm × 40 mm × 10 mm from a Ø45 mm round bar (Fig. 1c). The coatings were prepared in-house by HVOF (DJ Hybrid from Oerlikon Metco, Wohlen, Switzerland) and HVAF (M3 from Uniquecoat Technologies LLC, Oilville, USA) methods; the main spray parameters are given in Table 4. For HVAF, the medium pressure parameters were chosen, which are known (Ref 23) to produce a relatively dense coating and good deposition efficiency (DE) when using this powder. It should be noted that the HVAF M3 torch is pressure controlled and the fuel/air ratio is not known. In addition, the fuel/air control range is rather narrow and does not allow for a large influence on the coating properties. Therefore, it is common to vary the combustion chamber pressure level, from which is known that higher pressure produces higher gas flow velocity and thus higher particle velocity, and lower pressure produces longer dwell time and thus better melting and DE (Ref 23). In this work, a moderate pressure level was chosen to achieve good DE with HVAF. For the DJ Hybrid HVOF torch, the parameters recommended by the manufacturer were selected. These parameters were slightly over-stoichiometric (fuel-rich), which achieve the highest possible particle temperature, which is needed to produce a dense coating when using propane as a fuel gas.

Before the coating, the specimen surface was grit-blasted by using corundum particles with size between 500 and 700 µm to improve adhesion. As explained in the Introduction, the specimens were prepared with two different nominal coating thicknesses: 90 µm (HVAF only) and 300 µm (both HVAF and HVOF). It should be noted that only half of the specimen surface was coated in the axial direction, i.e., an area of 125 mm × 40 mm. The hardness of the sprayed coatings was measured with EMCOTEST hardness tester (EMCOTEST Prüfmaschinen GmbH, Austria) with 0.3 kgf load. The thinner coatings were left in the as-sprayed condition, whereas the thicker coatings were ground similarly to the plain steel specimens to a target thickness of 250 µm and roughness of Ra 0.2 µm measured in the longitudinal direction.

The residual stress states in the coatings produced by different coating methods were estimated using an

**Table 1** Chemical composition in wt.% of the substrate steel (EN 34CrNiMo6) according to manufacturer's data

C	Si	Mn	P	S	Cr	Ni	Mo	V	Cu
0.35	0.28	0.71	0.008	0.03	1.37	1.35	0.17	0.01	0.21

analytical model proposed by Tsui and Clyne Ref 38, which allows the calculation of in-plane stresses within the coating (and substrate) as a function of the distance from the interface. The model superposes the deposition stage quenching stresses (or peening stresses) caused by each individual coating layer and the post-deposition CTE (coefficient of thermal expansion) mismatch stresses formed during cooling of the sample from the deposition temperature to ambient temperature. In the present work, post-deposit CTE mismatch stresses were calculated using the actual geometry of the fretting specimens and the average temperature of the specimens during deposition. The temperature of the substrate was monitored during spraying using a Fluke Ti300 thermal imager (Everett, WA, USA). Temperatures during spraying ranged from 160 °C, which was the temperature at the start of each new pass, to 220–235 °C, higher when spraying with HVAF. Average substrate temperature used for calculations was 185 °C for HVOF and 195 °C for HVAF. CTE of  $12 \times 10^{-6} \text{ K}^{-1}$  was used for the steel substrate and  $5.2 \times 10^{-6} \text{ K}^{-1}$  (Ref 39) for the WC-CoCr coatings. To calculate the stresses generated in the coating during the deposition stage, information on the quenching (or alternatively the peening) stresses generated in each layer was required. Here, deposition stage stresses were determined using the iteration process by Tsui and Clyne Ref 40. In this process, the deposition stage stress used in the model is estimated by matching the calculated curvature of the coating with experimental data measured during the deposition process. The experimental curvature data for both HVOF and HVAF coatings were determined using a special measuring device (ReliaCoat Technologies, East Setauket, NY, USA), which measures the change in curvature of a 228.6 mm × 25.4 mm × 2.5 mm flat bar sample in situ during the spraying process (Ref 41). In addition to the original sources, the use of the procedure is described in more detail in references Ref 22 and Ref 42.

## Test Procedure

Table 5 lists the different contact configurations studied in this work. In order to facilitate straightforward comparison, identical test parameters were used for all the tests: bolt preload of 25 kN, nominal bulk bending stress amplitude of 180 MPa at the center of the bolt hole, and bulk loading

**Table 2** Mechanical properties of the substrate steel (EN 34CrNiMo6) according to manufacturer's data

Yield strength Rp 0.2, MPa	Tensile strength, MPa	Elongation A5, %	Reduction of area, %
990	1090	14	58

**Table 3** Nominal particle sizes and chemical composition (in wt.%) of the feedstock powders according to manufacturer's data

Powder	Method	Particle size, $\mu\text{m}$	W	Co	Cr	C	Iron(max)
Metco WOKA 3652	HVOF	15-45	Bal.	10.28	4.05	5.3	0.05
Metco WOKA 3654	HVAF	10-30	Bal.	10.25	3.82	5.4	0.04

**Table 4** Spray parameters of the HVOF and HVAF deposition processes

	HVOF	HVAF
Propane pressure, bar/psi	6.4	106
Propane 2 pressure, psi	...	105
Propane flow, L min <sup>-1</sup>	70	...
Oxygen flow, L min <sup>-1</sup>	238	...
Oxygen pressure, bar	10.3	...
Air pressure, bar/psi	7	108
Air flow, L min <sup>-1</sup>	375	...
Carrier gas, L min <sup>-1</sup>	20	60
Stand of distance, mm	220	300
F/O ratio	0.22	...
Total flow, L min <sup>-1</sup>	683	...
Powder feed rate, g min <sup>-1</sup>	40	100
Robot speed, mm s <sup>-1</sup>	950	950
Thickness/Pass, $\mu\text{m}$	15	14

frequency of 20 Hz. These parameters were selected based on an earlier work (Ref 12), which indicated fatigue life-time of  $\sim 1$ -2 million cycles for steel-to-steel contact. The contact pressure generated by the main clamping was 100 MPa, i.e., sufficiently high so that the clamping could be considered rigid. The test series involved tests run until failure and interrupted tests run up to 1000, 10,000, or 100,000 cycles. Specimen failure was detected based on the strain gauge readings; when the fatigue crack propagated across the thickness of one of the specimen halves, the stiffness of the specimen changed, which was seen as changes in the corresponding strain amplitudes. All the tests were performed without any lubrication between the carefully pre-cleaned contact surfaces. After the fretting tests, the specimens were cleaned with ethanol in an ultrasonic cleaner and the contact surfaces were inspected with optical and scanning electron microscopes (SEM). Crack initiation and propagation were studied using cross-

sectional samples prepared from the most severely damaged regions of the specimens. For this, specimens were cut parallel to the axial direction, mounted in epoxy resin and polished prior to the SEM inspection, in which both secondary electron (SE) and backscattered electron (BSE) imaging modes were used.

### Finite Element Method Simulations of the Experiments

As noted above, implicit FEM simulations running on Dassault Systems SIMULIA Abaqus/Standard R2017x were used to calculate the distributions of stress and slip at the contact interface between the specimens. For this, the methodology developed by Juoksukangas et al. Ref 12 was adopted. In short, the simulation model (Fig. 1b) involved the main components of the experimental setup, i.e., the two specimens, the bolt and the spacers, as well as the two pads of the main clamping. Due to symmetry, only half of the setup was modeled. The specimens were modeled using C3D8I continuum elements with a nominal element size of 1 mm at the contact region of interest. Similarly to the earlier study by Juoksukangas et al. Ref 12, the contact between the specimens was modeled with a master-slave surface-to-surface algorithm, which used penalty contact with elastic slip of  $0.05 \mu\text{m}$  and a Coulomb friction model for the tangential direction and an Augmented Lagrange "Hard contact" formulation for the normal direction. The COF between the specimen surfaces has a notable effect on the fretting behavior, especially on the location of the most severe fretting damage (Ref 12), which, as discussed later in the Results section, is used to deduce the value of COF in the studied cases by comparing the simulation predictions (distribution of frictional work on the surface) with experimental observations of the fretting surface damage. The same type of contact formulation was used also for other parts of the setup with a constant COF 0.6. The steel material was modeled with a linear elastic material model



**Table 5** Contact configurations of the experimental study

Surface 1	Surface 2	Loading cycles
HVAF coating, thickness 90 $\mu\text{m}$ , as-sprayed (Ra 3.3 $\mu\text{m}$ )	Steel, ground Ra0.2 $\mu\text{m}$	1000, 10,000, 100,000, up to failure ( $1.33 \times 10^6$ )
HVAF coating, thickness 250 $\mu\text{m}$ , ground Ra 0.2 $\mu\text{m}$	Steel, ground Ra 0.2 $\mu\text{m}$	1000, 10,000, up to failure ( $1.71 \times 10^6$ )
HVOF coating, thickness 250 $\mu\text{m}$ , ground Ra 0.2 $\mu\text{m}$	Steel, ground Ra 0.2 $\mu\text{m}$	1000, 10,000, up to failure ( $1.86 \times 10^6$ )
HVAF coating, thickness 250 $\mu\text{m}$ , ground Ra 0.2 $\mu\text{m}$	HVAF coating, thickness 250 $\mu\text{m}$ , ground Ra 0.2 $\mu\text{m}$	10,000, up to failure ( $1.03 \times 10^6$ )

The last column indicates the tests carried out (interrupted tests and tests up to failure)

using Young's modulus and Poisson's ratio of 206 GPa and 0.28, respectively. In the current study, the coating was introduced to the simulation model as an additional layer of elements with corresponding thickness (90  $\mu\text{m}$  and 250  $\mu\text{m}$ ). Similarly to the steel substrate, linear elastic model with Young's modulus of 300 GPa (Ref 2, 22, 23, 43) and Poisson's ratio of 0.3 was used for the coating elements. Damage and failure effects (including interfacial failure) as well as residual stresses were excluded from the model. This simplification was considered justified since the main purpose of the simulations was to obtain continuum level estimates for the contact parameters (stress and slip) to support the analysis of the experimental data.

The boundary conditions of the simulations were set so that the main features of the experimental setup could be modeled with relative simplicity. The bolt was tied to the spacers, which themselves were in contact with the specimen surfaces based on the contact formulation described above. The bolt preload was applied directly using the "bolt load" feature of Abaqus. The lower end of the main clamping was fixed, whereas a clamping pressure of 100 MPa was applied on the upper part of the main clamping similarly to the experiments. Finally, bulk loading was introduced by applying a displacement boundary condition at the free end nodes of the two specimens. In the simulations, three bulk loading cycles were run and the results were post-processed and analyzed in terms of stresses in the specimens and frictional work at the contact interface.

## Results and Discussion

In the following, the main results and findings of the study are presented and discussed. The presentation is started by an analysis of the sprayed coatings, followed by a comparison between the fretting experiments and the continuum simulation predictions, after which a detailed analysis of the microscale phenomena occurring during fretting is presented.

## Coating Characteristics

The measured  $HV_{0.3}$  hardness of the coatings was  $1180 \pm 23$  and  $1113 \pm 89$  for the HVOF and HVAF coatings, respectively. These values are quite typical for this coating type (e.g. Ref 2, 8, 22, 23, 43, 44). The microstructures of the coatings are shown in Fig. 2 at a detailed level. The carbides in the coatings, which appear light gray in Fig. 2, are about 1  $\mu\text{m}$  in size. The difference between the two spraying methods is highlighted by the fact that, as a result of carbide dissolution during spraying, the carbides in the HVOF coating are slightly rounded at the edges and very small carbides are missing. In the HVAF coating, in contrast, the carbides are sharp-edged and sub-micron size carbides are also present. The dissolution of tungsten and carbon into the matrix is known to make the matrix more brittle, and since it is greater in the HVOF coating, it is expected that the behavior of the HVOF coating is more brittle compared to the HVAF coating.

The through thickness stresses in the samples according to Tsui and Clyne's analytical model Ref 38, 40 are shown in Fig. 3. The HVAF method generates a compressive stress of about 300 MPa in the coating, while the HVOF method generates a tensile stress on the surface of the coating, which becomes a compressive stress as it moves toward the substrate. The difference is logical considering the flame temperature, which is much lower in the HVAF process compared to HVOF process. Due to the melting degree of the powder particles in the HVAF process, during the deposition stage, the peening effects, which generate compressive stresses, are stronger, whereas in the HVOF process the dominant stresses are quenching stresses, which are always tensile stresses (Ref 22). When the coating cools down after the coating phase, the relatively large CTE difference between the coating and the substrate shifts the stress state of both coatings toward net compressive stress.

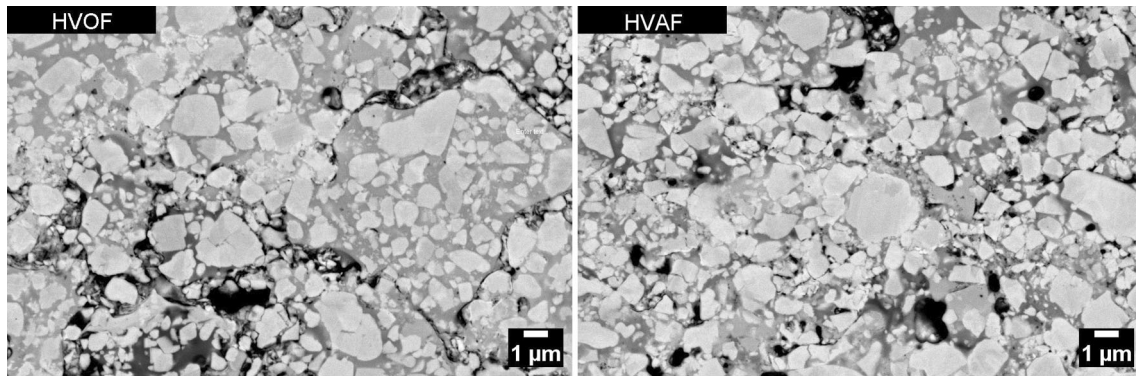


**Fig. 2** High-resolution SEM (backscatter electron) micrographs of the HVOF and HVAF sprayed coatings

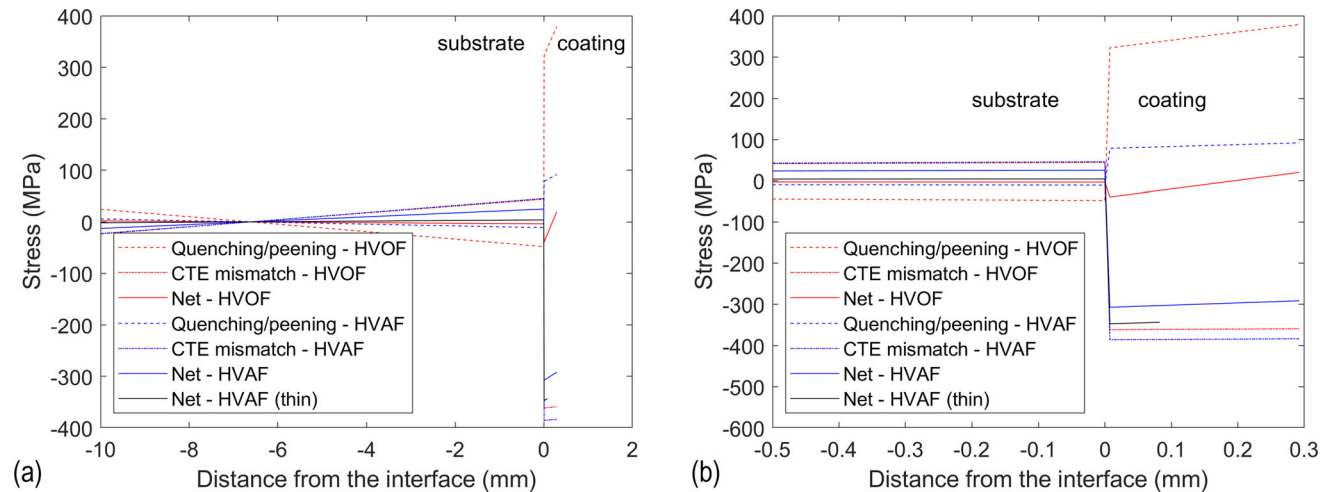


**Fig. 3** In plane stresses at different depths according to the Tsui and Clyne analytical model: (a) full specimen thickness and (b) zoom-in of (a) near the coating/substrate-interface

### Macroscopic Damage and Fatigue Life

As noted earlier, after the fretting tests, the contact surfaces of the specimen halves were carefully examined using optical and scanning electron microscopes. After this cross-sectional samples were prepared and examined. The analysis of the fretting damage mechanisms was based on qualitative assessment of the optical and SEM images. In the following, the main findings of the characterization are discussed alongside with the numerical simulation results. Figure 4 presents examples of the evolution of the fretting damage in (thin) coating-to-steel contact and (thick) coating-to-coating contact. Here, it is emphasized that each presented cycle number involves a new specimen pair; that is, once the test was interrupted and the two specimens were separated from each other, the same pair was not reloaded. As illustrated in Fig. 4(a), similar fretting scar developed on the coating and steel contact surfaces. Notable amount of reddish-brown wear debris consisting mainly of steel particles was formed during the fretting

process. In addition, detached carbides and coating fragments were observed on the contact surfaces in the wear debris layer. A similar phenomenon was observed in all coating-to-steel contact pairs. As shown in Fig. 4(a), the fretting damage in both specimen surfaces increased as the number of loading cycles increased, but some degree of fretting damage was already observed after 1000 cycles. Furthermore, the amount of adhesive wear and material transfer between the specimen surfaces increased significantly between 10,000 and 100,000 cycles. In the coating-to-coating case, in Fig. 4(b), in contrast, indications of adhesive wear in terms of cold welds were less frequent and the color of the wear debris changed from reddish-brown to black. In addition, the location of the most severe damage region moved somewhat closer to the bolt hole compared to the coating-to-steel cases. However, in both cases the final fracture of one of the specimen halves took place within the most damaged region. The cracking behavior is discussed in more detail later in conjunction with the simulation results.

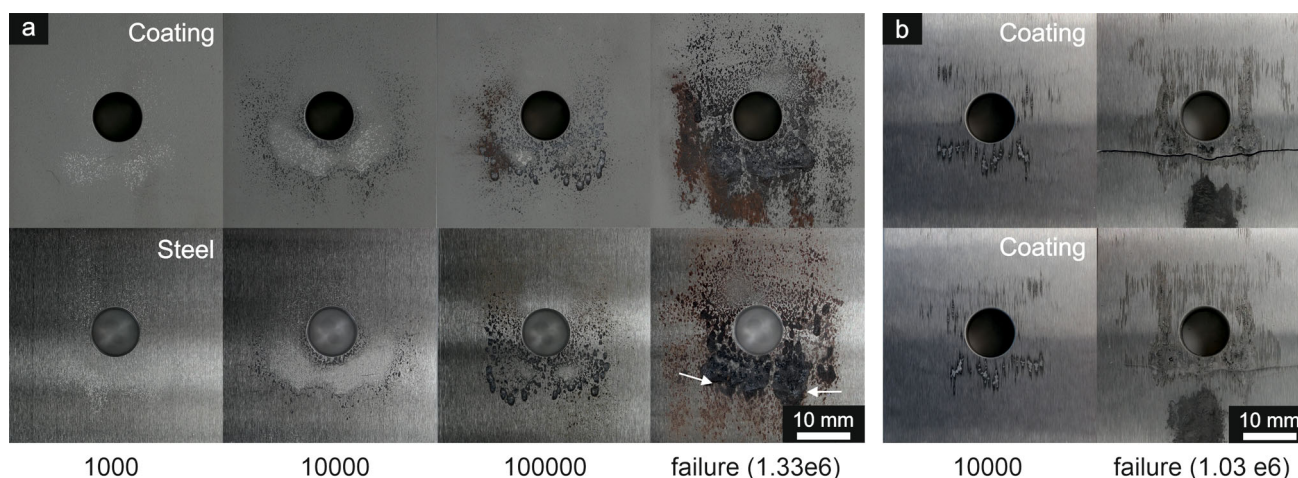


**Fig. 4** Evolution of the fretting damage on the contacting specimen surfaces, (a) from left to right, thin and rough HVAF (upper row) against steel loaded until 1000, 10,000, 100,000, and  $1.33 \times 10^6$  cycles (failure), (b) thick and ground HVAF coating-to-coating pair loaded until 10,000 cycles and  $1.03 \times 10^6$  cycles (failure). The scale

bar has a length of 10 mm and is the same for all images. The location of the fracture in the steel specimen in (a) is marked by arrows. The longitudinal specimen axis is vertical in the figures with free end pointing toward the bottom of the page

In general, the location of the main fretting scar on the contact surface was similar to the earlier study on steel-to-steel contact (Ref 12), according to which the frictional dissipation at the interface can be used to numerically predict the intensity of the fretting damage. The use of the frictional work as damage indicator is also supported by the work by Leidich et al. Ref 45, who used the accumulated friction energy in the prediction of fretting wear damage in flat annular contacts involving different coatings (DLC, solid film lubricant) against QT steel. In addition, more sophisticated damage analyses, such as the strain energy density-based methods used recently by Zeng et al. Ref 36, require a number of calibration parameters, which were not available in the current study. Therefore, frictional dissipation at the contact interface was used as the main numerical damage indicator in the current study. It should, however, be noted that the used approach gives only an indication of the location of the most severe damage but does not predict the amount of damage nor the specimen lifetime. Furthermore, as discussed later in more detail, the simulations provide only continuum estimates of the field variables, such as stress, and hence cannot be used to predict localized phenomena, such as adhesion spots. On the other hand, the used simulation approach can be considered typical in engineering design, and therefore, it is valuable to compare its predictions with the experiments.

As noted above, the main simulation parameter affecting the distribution of the frictional dissipation is the coefficient of friction; the effects of coating thickness and the type of contact (coating-to-steel versus coating-to-coating) were found to be small in the used simulation approach. Figure 5(a) shows examples of the simulated frictional dissipation for different COF in the case of coating (250

$\mu\text{m}$ )-to-steel contact (additional data, i.e., contact surface pressure as well as shear stress and slip on the contact surface are presented in Appendix). As can be seen in Fig. 5(a), for a low value of COF (0.3) notable frictional dissipation takes place on a wide area surrounding the bolt hole, whereas with higher values of COF (0.6 and 0.8) frictional work is concentrated on an area extending up to a distance of  $\sim 10$  mm from the hole edge toward the free end. Comparison with experimental data (Fig. 4) indicates that the main fretting scar location can be predicted well in the coating-to-steel case with a high COF ( $\sim 0.8$ ). This estimated value of COF is in good agreement with previous reports for hardmetal coating-to-steel contacts; Kubiak et al. Ref 32, 33 reported a value of  $\sim 0.7$ , whereas according to Okane et al. Ref 34 the COF is low ( $\sim 0.3$ ) at the start of loading but increases to 0.6–0.8 as the number of cycles increases. In these previous studies, the coatings were prepared with HVOF process, but the results of the current study indicate similar behavior in HVAF coatings. It is also noteworthy that the application of the hardmetal coating on one of the contact surfaces seems to have a small reducing effect on the COF compared to the steel-to-steel case. This has been reported earlier (Ref 31–34) and can also be deduced by comparing the current data to earlier studies on the same steel alloy in uncoated state. (Both Juoksukangas et al. Ref 12 and Hintikka et al. Ref 37 reported steady-state COF values between 0.8 and 1.0 for the steel-to-steel contact.) In the coating-to-coating case (Fig. 4b), in contrast, the fretting damage takes place closer to the hole, which implies that the COF is somewhat lower.

Figure 5(b) presents the axial tensile stress field in the coating at the moment of maximum bending displacement. Due to the symmetric bulk loading, in general the



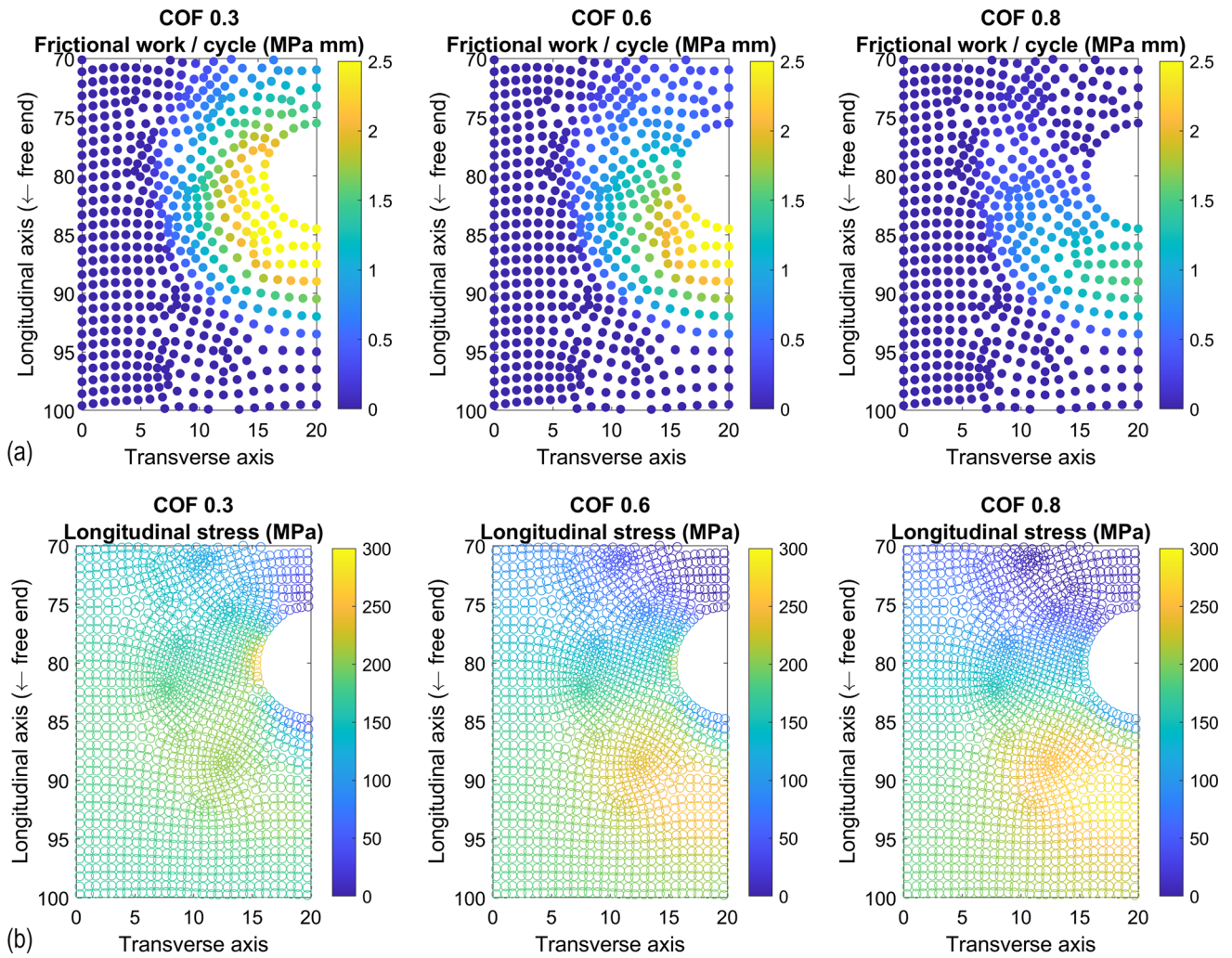


**Fig. 5** Simulated field data for the 250  $\mu\text{m}$  coating-to-steel contact case, (a) calculated frictional work (per unit area) at the contact interface (per cycle) and (b) axial stress in the coating at the moment

of maximum bending displacement. The rows correspond to interfacial COF of (i) 0.3 (ii) 0.6, (iii) 0.8

maximum tensile stresses correspond also to the cyclic stress amplitude (i.e., local mean stresses are close to zero). As can be seen, the simulation data indicate that high local tensile stresses, up to  $\sim 300$  MPa, appear within the coating in the same region as the frictional dissipation on the surface. Corresponding stress field is also formed in the steel counterpart with generally lower stress level (maximum near 200 MPa) due to the difference in the Young's moduli between the coating and the steel. In the tests run until failure the locations of the final fracture were the following (fracture location measured as the distance between the fracture and the edge of the hole on the centerline): in the thin and rough HVOF coating-to-steel contact (Fig. 4a) 6.1 mm, in the thick and ground coating-to-steel contact 9.7 mm (HVOF) and 5.1 mm (HVOF), and in the coating-to-coating contact (Fig. 4b)  $\sim 3$  mm. Comparison of this data with the simulations indicates that

the final fatigue fracture took place within the area associated with major frictional dissipation and high axial stress amplitude. The relatively high tensile loading might contribute to the damage process of the (brittle) coating also in the absence of fretting-induced surface damage. Based on the experimental characterization, in general the coatings did not crack outside the main fretting damage area. However, in the coating-to-coating case some minor cracking was observed in the test interrupted after 10,000 cycles in the vicinity of the specimen edges close to the main fretting scar. The cracking tendency of the coatings in the studied loading conditions is discussed later in more detail.

A somewhat surprising observation is that in all tested cases, the number of cycles until failure (Table 5) was in the same order of magnitude as reported earlier for steel-to-steel contact in similar loading conditions (Ref 12).

Therefore, the previously reported Ref 33, 34 increase in fretting fatigue strength via application of the hardmetal coating was not observed in the current study. This can be related to at least two differences between the current work and the previous reports. Firstly, in the previous studies bulk fatigue loading was imposed only on the coated counterpart of the contact, whereas in the current study symmetric bulk loading was applied, which led to fatigue failure of the uncoated side. Secondly, in the previous studies the contact loading geometry (sphere/pad) was such that the fretting loading was concentrated on a very small section of the specimen surface, whereas in the current study the effective fretting damage area was relatively large. This increases the chance that a potentially weak location of the coating microstructure is subjected to detrimental loading. Furthermore, as discussed later in detail, the large contact area promoted the development of large adhesion spots (Ref 37), which are directly related to specimen failure. It should, however, be noted that since the current study focused on the analysis of the microscale phenomena, the number of specimens run until failure is modest and the present results on the total fatigue lifetime should be considered only indicative.

### Microscopic Surface Phenomena

Detailed inspection of the damaged surfaces revealed that in all of the coating-to-steel cases adhesion contact spots and cold weld regions were readily formed. This was especially evident in the case of the thin as-sprayed (rough) HVAF coating-to-steel pair, where adhesion spots were also observed away from the most severely damaged area. These asperity contacts led to sheared dents on the surface of the steel specimen already after 1000 cycles. In general, the amount of adhesive contacts increased with increasing number of cycles and the location of the primary crack in the steel specimen was strongly related to the adhesion spots, as shown in Fig. 6(a). This finding is in correspondence to the previous study by Nurmi et al. Ref 46 on the same steel alloy in steel-to-steel fretting contact, in which fatigue crack nucleation was related to localized accumulation of plastic strain at the adhesion spots. As can be seen in Fig. 6(a), the adhesion spots affect locally the direction of the crack; in the coating-to-steel contacts, the primary cracks leading to specimen failure were observed to follow the edges of the most severe adhesion spots where the local stresses are assumed to reach the highest values. Even though this kind of a local phenomenon cannot be simulated with the used continuum-scale FEM methodology,

the evidence of strong adhesion spots supports the view that the coating-to-steel contact is associated with a high coefficient of friction.

It should be noted that cracks and material removal via carbide detachment were observed in the coatings in all studied cases. The surface damage on the coating is exemplified in Fig. 6(b) for the case of thick and ground HVAF coating against steel. This kind of fretting wear of the hardmetal coating was reported also by Wang et al. Ref 35, and it indicates that in the present study the imposed (total) loading was larger than the possible crack nucleation threshold of the coating proposed earlier by Kubiak et al. Ref 32, 33. In the current study, detached wear debris entrapped between the contact surfaces was observed to generate abrasive wear as the number of loading cycles increased. In particular in the coating-to-coating case abrasive wear seemed to be dominant, since the surfaces were more pitted. Some adhesive cold welds, which also affected the local direction of the cracks, were observed, but not to the same extent as in the coating-to-steel cases. Overall, the contact surfaces of the coating-to-coating specimens loaded until failure were strongly abraded as shown in Fig. 6(c).

The different contact cases (coating-to-steel versus coating-to-coating) differed from each other also in terms of the formation of a third body layer (TBL). The formation of a layer of wear debris to at least some degree was observed on all of the contact surfaces of the coating-to-steel cases. Particularly in the case of thin as-sprayed (rough) HVAF coating against steel a thick third body layer was observed on the coated specimen, as shown in Fig. 6(d). In this case, the high surface roughness of the coating leads to greater amount of wear debris originating mainly from the steel surface, as the adhesive contacts shear and deform during the fretting process. However, EDS analysis made on the steel counterpart (data presented in Appendix) revealed traces of tungsten on the surface layer, which shows that damage and particle detachment on the coating also contributes to the development of the contact. The wear debris layer (third body layer) modifies the contact conditions and can play a major role in fretting wear behavior since it can affect the wear rate (Ref 35, 47, 48). In some cases, it has been reported that oxidized TBL could act as a protective layer against fretting damage on contact surfaces and reduce the wear rate (Ref 49, 50). However, in this study the TBL did not seem to affect the fretting fatigue life, since the primary cracks in the steel specimens nucleated due to the adhesive contacts. Furthermore, in the coating-to-coating contact the

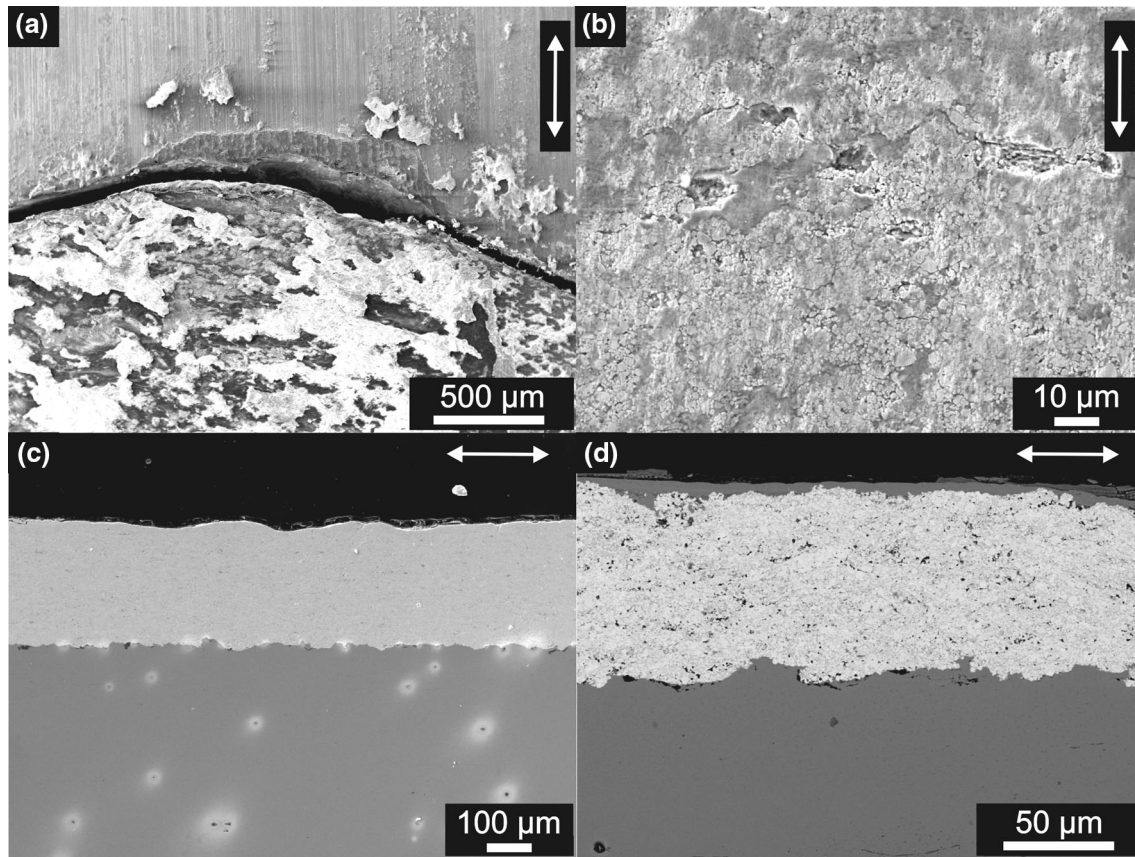


**Fig. 6** (a) Adhesion spot and primary crack in a steel specimen against thick and ground HVOF coating (specimen pair loaded until failure), (b) material removal and cracks in a thick and ground HVOF coating against steel (specimen pair loaded until failure), (c) surface degradation of thick and ground HVAF coating in coating-to-coating

contact (specimen pair loaded until failure), and (d) third body layer on the thin and rough HVAF coating against steel specimen (specimen pair loaded until failure). The slip direction is marked by the arrows

dominant wear mechanism seems to be more abrasive in nature, characterized by the wear product between surfaces acting as a surface degradation agent.

### Observations on the Specimen Cross-Sections

Based on the characterization of the cross-sectional samples, cracks were mainly initiated at the contact surface and propagated toward the inside of the specimen perpendicularly to the slip direction, i.e., in mode I with respect to the bulk bending stress. In addition, some subsurface cracks were formed in the case of thick HVOF coating against steel. Furthermore, the adhesion between the coatings and the steel substrate was good, since interface damage such as delamination was not observed. The implications of this finding are discussed later in Sect. “Summary”.

The cracks were concentrated at the areas of the most severe fretting damage, and in the specimens loaded until

failure the major cracks were formed in the corresponding (mirroring) locations of the contacting specimen surfaces. Thus, it cannot be excluded that the formation of a crack on one surface induced a stress concentration on the other surface and led to crack nucleation on that side too. It is noteworthy that in the case of thick coatings against steel, cracks were found in the coatings already after 1000 cycles despite the fact that the final failure took place in the steel counterparts. After 1000 cycles the crack length was about 50  $\mu\text{m}$  in both thick coatings, while after 10,000 cycles the average crack length remained in the same range, and the maximum crack depth was less than half of the coating thickness in both thick coatings. In contrast, in the steel counterpart in contact with the thick HVOF coating cracks were observed only after 10,000 cycles, while in the steel counterpart in contact with the thick HVAF coating cracks were not found in the interrupted tests, i.e., crack formation seemed to require more than 10,000 cycles. In the case of



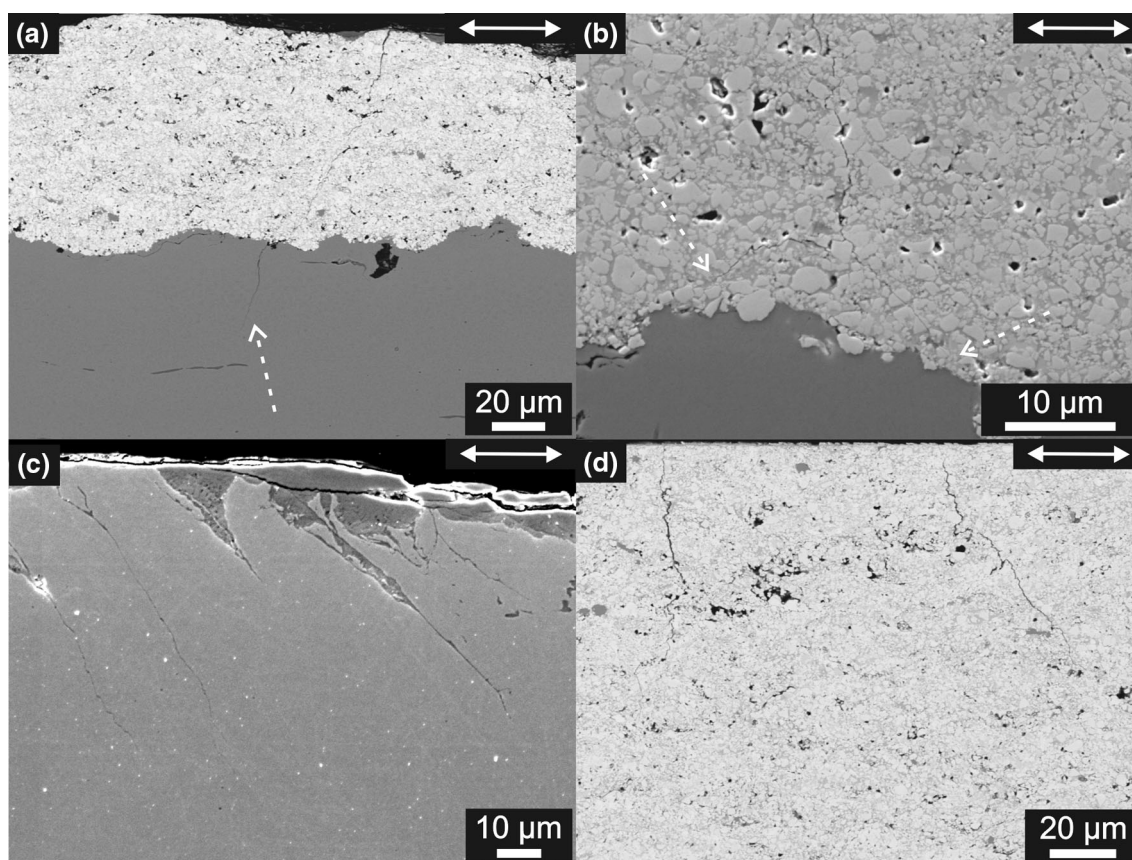


**Fig. 7** (a) Primary crack (marked with dotted arrow) propagated from the coating to the base material in the case of thin and rough HVOF coating against steel (specimen pair loaded until failure), (b) crack tip (marked with dotted arrows) in thick and ground HVOF coating against steel (specimen pair loaded until failure), (c) cracks in steel

specimen against thick and ground HVOF coating (specimen pair loaded until failure), and (d) cracks in the thick and ground HVOF coating in the case of coating-to-coating contact (specimen pair loaded until 10,000 cycles). The slip direction is marked by the arrows

thin and as-sprayed (rough) HVOF coating against steel, surface inspection after 10,000 cycles revealed micrometer-scale crack-like surface traces on the steel surface and material detachment on the coating surface in the vicinity of adhesion spots. However, cracks were not observed in the cross-sectional samples taken from either side in the interrupted tests, i.e., crack formation required more than 100,000 cycles. Overall, in the coatings the cracks seemed to initiate earlier than in the steel counterparts but the propagation until failure was delayed compared to the steel. The apparently slower crack propagation rate in the coated side is in accordance with previous studies (Ref 33, 34). The crack growth in the coatings in this case may also be retarded by the fact that, due to the low CTE of the coating material, both coatings are eventually under compressive stress in the vicinity of the substrate, as shown in Fig. 3. However, the large difference in the magnitude of the residual compressive stress between the coatings

( $\sim 300$  MPa in HVOF versus  $\sim 30$  MPa in HVOF) seems to have almost no effect on the depth of cracks in the coatings.

In all the coating-to-steel specimens loaded until failure, the steel counterparts fractured completely, whereas the coated specimens remained whole. However, in the case of thin HVOF coating against steel, a crack in the coating had propagated to the substrate steel, as shown in Fig. 7(a). It is therefore evident that in this case failure of the coated specimen side was also a likely possibility. In the case of thick coatings against steel, relatively large cracks were observed, but in all cases the cracks were stopped latest at the interface of the coating and the substrate steel, as exemplified in Fig. 7(b).

In the coating-to-steel cases, the cracks observed in the coatings were initiated at the highest points of the surface structure, i.e., at the locations of adhesive contact with the steel counterpart. In the steel specimens, in addition to the



**Table 6** Summary of the damage mechanisms in different contact pairs

Contact case	Main surface damage mechanism	Main fatigue mechanism
Steel-to-steel	Adhesive wear	Crack nucleation at adhesion spots
Coating-to-steel	Adhesive wear on both surfaces	Crack nucleation at adhesion spots on both surfaces; early nucleation in the coating, but faster propagation and final failure on the steel side
Coating-to-coating	Mainly abrasive, some adhesive	Crack nucleation at the abraded surface of the coating, propagation to substrate steel

The steel-to-steel case is deduced based on previous literature reports Ref 12, 37, 46

primary fracture, notable number of shorter cracks were formed, as shown in Fig. 7(c) for a steel specimen against thick and ground HVOF. In the coating-to-coating specimen pair loaded until failure, in addition to the primary fracture, several secondary cracks had propagated from the coating to the substrate steel. Compared to the case of coating-to-steel contact, the cracks in the coating-to-coating case were strongly opened, and fragments had detached from the surface at the crack nucleation spots. Already after 10,000 cycles, the coated surfaces were heavily cracked, and the cracks had grown to a depth of about 50 micrometers, as illustrated in Fig. 7(d). Wang et al. Ref 35 proposed in their study that in suitable loading conditions abrasive wear could slow down the formation of fretting fatigue cracks by wearing out the microcracks. It appears that in the current study this mechanism was not significant enough to affect the total lifetime, since especially in coating-to-coating cases, strong abrasive wear and the formation of detrimental fatigue cracks took place simultaneously. The crack growth in the coatings appears to be driven by their relatively high defect density and brittleness, which promotes both abrasive wear and fatigue crack propagation.

## Summary

In the following, a short summary of the fretting behavior of contacts involving WC-Co-Cr hardmetal coatings is presented with emphasis on the technological implications of the observations. Table 6 summarizes the surface damage and fatigue mechanisms of the two main contact cases studied in this work, coating-to-steel and coating-to-coating, and compares them to the steel-to-steel reference case taken from the literature (Ref 12, 37, 46). As discussed above, the application of the coating on one or both of the contact surfaces had little influence on the total fatigue

lifetime of the studied bolt joint. This observation is somewhat in contrast with previous reports (Ref 33, 34), according to which the application of the hardmetal coating should increase the fretting resistance of the steel surface. However, in the previous studies fatigue-inducing bulk loading was imposed only on the coated side of the joint and not on the counterpart. Thus, in the current study, where symmetric loading was applied, the results of the coating-to-steel case can be readily explained by the failure of the uncoated side, where crack nucleation took place similarly to the steel-to-steel case at adhesion spots formed on the contact surface. It is, however, noteworthy that notable damage, such as surface cracking and carbide detachment, was observed also in the coatings. In fact, deep ( $\sim 50 \mu\text{m}$ ) cracks were observed to form first in the coatings, even though faster crack propagation in the uncoated steel side did lead to final failure on that side. Therefore, the hardmetal coating cannot be assumed to act as a hard, slowly wearing, counterpart against the steel.

In the second studied case, coating-to-coating, surface damage was dominated by abrasive wear with less indications of adhesion between the surfaces. Similarly to the coating-to-steel case, relatively deep cracks formed early in the coatings. It is known that in plain fatigue the application of a hardmetal coating can reduce the fatigue limit of a high-strength steel (e.g. Ref 5, 28). It thus appears that in the studied joint the rapid crack formation in the coating led to a situation, where the coating was acting more to reduce fatigue endurance of the underlying substrate via propagation of cracks from the coating to the substrate than to provide protection against surface damage. A necessary condition for this mechanism is that the adhesion between the substrate and the coating is high enough so that delamination does not occur when the crack in the coating reaches the interface (Ref 25).

As noted above, coating delamination was not observed in the current experiments. This finding is in line with

previous literature reports, according to which the occurrence of the coating delamination is case-specific. For example, in the case of cylindrical WC-CoCr-coated (HVOF) steel specimens subjected to rotating bending fatigue, Vackel and Sampath Ref 25 reported that no delamination of the coating took place except for the final fracture site, where it was related to notable substrate deformation. Barbera-Sosa et al. Ref 28 reported that under axial cyclic loading of a 50% WC-10Co-4Cr/50% Colmonoy 88 (HVOF) coating deposited on QT steel (SAE 4340), fatigue cracks in the coating could cause delamination at the interface, when defects, such as embedded alumina particles from the grit blasting, were present. Gui et al. Ref 51 studied the effect of coating thickness on the transverse cracking and delamination (spallation) during axial bending in the case of WC-10Co-4Cr (HVOF) coating on an ultra-high-strength 300 M steel. They noted that as the coating thickness was increased from 80 to 275  $\mu\text{m}$ , the transverse cracking tendency of the coating decreased, whereas the tendency toward delamination increased. This was explained in terms of transverse cracking and delamination acting as complementary mechanisms to accommodate the imposed deformation in the coating. A similar approach was used to explain delamination during axial fatigue tests (Ref 51).

Based on static measurements, Agüero et al. Ref 5 reported that the adhesive strength of a WC-Co-Cr (HVOF) coating on a 4340 low alloy steel is above 89 MPa. (The exact value could not be determined as delamination did not take place in their bending test.) According to the FEM analysis carried out in the current study, the maximum shear stress on the fretting contact surface is  $\sim 80$  MPa, i.e., below the adhesive strength reported in Ref 5. Even though continuum-scale FEM analysis might be too coarse to estimate the local stress state at the coating/substrate-interface, the results are in agreement with experimental evidence. Thus, it can be concluded that coating delamination did not take place in the studied fretting loading conditions.

Finally, it is useful to briefly consider the obtained results from the viewpoint of the coating fracture toughness. Based on the work by Schulze and Erdogan Ref 52, for this coating-substrate system, where the elastic moduli differ relatively little from each other, the mode I stress intensity factor for the coating cracks can be estimated by the well-known solution for single edge crack:  $K_I \approx f\sigma_0\sqrt{\pi a}$ , where  $\sigma_0$  and  $a$  are the applied stress and crack length, respectively. The constant  $f$  obtains values between 1.12 and 1.25 for crack lengths 0... 80% of the coating thickness, when the ratio of the coating to substrate shear modulus is 0.6 (Ref 52). Thus, based on the FEM

prediction of 300 MPa external tensile loading, for the  $\sim 50$  to  $\sim 100$   $\mu\text{m}$  long coating cracks, which appeared already between 1000 and 10,000 cycles in the thick coatings, the stress intensity factor is between  $\sim 4$  and  $\sim 7$   $\text{MPa}\sqrt{\text{m}}^{1/2}$ . These values are of the same magnitude as the typically reported fracture toughness values for this type of coating (Ref 2, 8, 22, 23, 43, 44). On the other hand, the stress intensity factor of a crack decreases rapidly, when multiple cracks are formed periodically close to each other (e.g., if the crack spacing is twice the crack length, the stress intensity factor is reduced by  $\sim 50\%$  compared to the case of a single crack (Ref 52)). Multiple cracks forming close to each other were indeed observed in the current study (e.g., Fig. 6(b) and 7d)). Furthermore, especially in the coating-to-steel contact case adhesive contact spots formed between the surfaces. The applied FEM methodology does not allow for the calculation of local stresses in the adhesive spots, but it can be assumed that the continuum value (300 MPa) represents a lower-bound estimate. Hence, it is plausible that the early formation of coating cracks, which coincides with the formation of adhesive junctions, acts to relieve the high local stresses in the coating. That is, the local deformation and stress gradients near the vicinity of the adhesion spots are accommodated by localized cracking in the (relatively) brittle coating and by local plastic deformation in the steel counterpart. Under bulk cyclic loading the once formed cracks in the coating open and close cyclically, but their maximum length remains relatively constant. In contrast, on the steel side localized cyclic plastic deformation leads to the nucleation and growth of the fatigue crack which causes macroscopic failure. This would at least qualitatively explain the observation that the early cracking in the coating is followed by final failure on the uncoated side. However, this analysis does not lead to quantitative predictions of the specimen lifetime in different contact cases. Similarly, the observation, that the coating residual stress state (HVOF versus HVAF) does not considerably affect the cracking behavior, is not explained by this approach. Thus, further analysis, which is beyond the scope of the current work, is needed on the topic.

## Conclusions

This study focused on the effects of thermal sprayed WC-10Co-4Cr hardmetal coating on the fretting behavior of a bolt joint. The substrate material as well as the counterpart material was quenching and tempering steel 34CrNiMo6. The coatings were deposited by HVOF and HVAF methods using WC-Co-Cr powder. Coating-to-steel and coating-to-

coating contact conditions were studied with a cantilever beam type test setup, which imposed the same bulk cyclic loading on both contacting parts. Both interrupted tests and tests until failure were carried out. After the tests, the failure mechanisms were analyzed by characterization of surface damage and cross-section samples using optical and scanning electron microscopy. Continuum-scale linear elastic finite element method calculations were used to predict the location of fretting damage in terms of frictional work and axial stresses using different values of the coefficient of friction (COF).

The following conclusions were made:

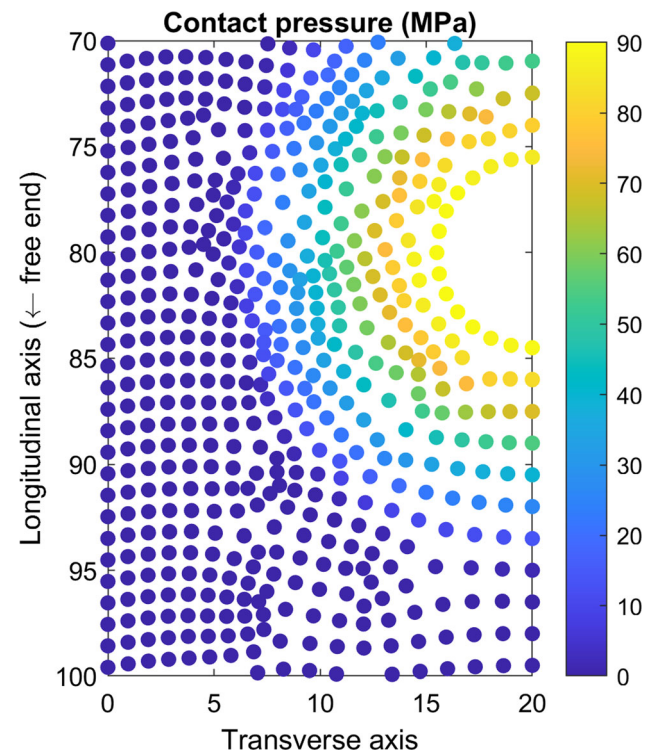
1. The applied test methodology was found feasible for the fretting tests of coated materials. Due to the symmetric loading, fatigue failure will take place on the side (either coated or uncoated), which has lower fretting fatigue endurance. Therefore, the used approach is suitable for the evaluation of the total fretting fatigue performance of a given contact pair.
2. In the studied bolt joint, the application of the hardmetal coating does not seem to considerably affect the total fatigue lifetime of the joint when compared to steel-to-steel contact. Also, the coating deposition method (HVOF versus HVAF) does not seem to have an effect in the studied loading conditions.
3. In all fretting tests, some degree of fretting damage took place in both counterparts and it increased with increasing number of loading cycles
  - In coating-to-steel contacts, the main surface damage mechanism is adhesive wear: notable amount of adhesive contact spots and cold welds form on the damage area, material removal takes place in both counterparts and a third body layer forms on the surface.
  - In coating-to-coating contact, abrasive wear is dominant, which leads to severe surface degradation. This was related to the hard wear product that promotes further wear of the surfaces. In addition, some adhesive contact spots form also in this case.
4. In general, cracks were observed to form earlier in the coatings than in the steel counterparts, but the cracks in steel propagate faster to cause the final failure on that side. As a result, the total fatigue lifetime of the joint does not notably differ from the steel-to-steel case. Secondary cracks were found in addition to the primary crack both in the coatings and in the steel counterpart.
5. In the coating-to-steel case, the main crack in the steel counterpart was observed to follow locally the edges of the adhesive contact spots, where the local stresses are assumed to reach their highest values.

Based on the results of the current study, it is evident that if a given coating is considered as a potential fretting fatigue palliative in a mechanical joint, the fatigue behavior of both counterpart surfaces should be carefully studied. In many cases this calls for more experimental work, since typically fretting fatigue is studied by applying bulk loading on only one of the counterpart surfaces. In addition, in the case of hardmetal coating-to-steel-contacts studied here, further work should be focused on the formation mechanisms of the local adhesion spots, which induce localized cracking in both the coating and in the steel counterpart and thus create potential nucleation sites for macroscopic fatigue cracks.

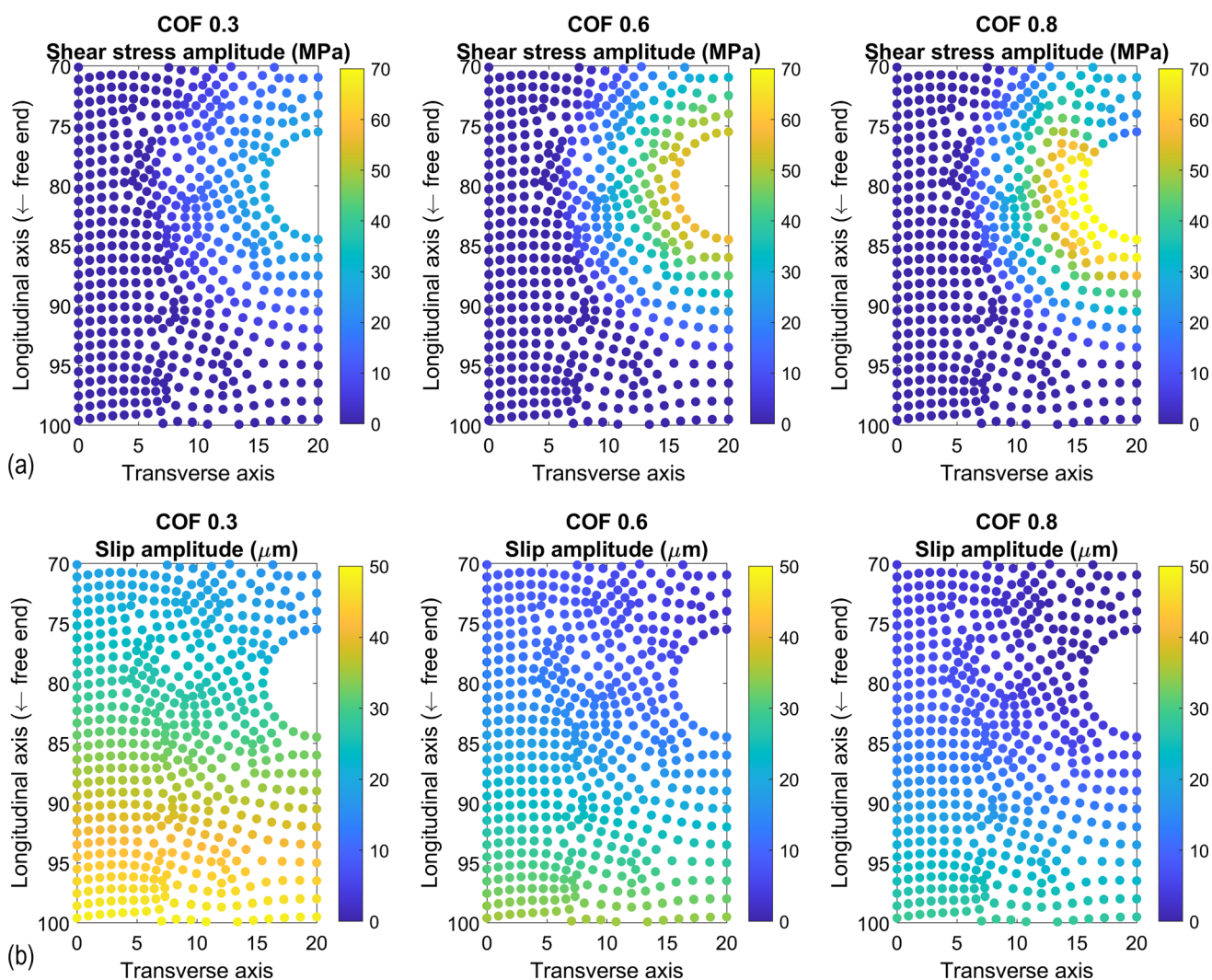
## Appendix

Figure 8 and 9 presents the simulated contact pressure as well as shear stress and slip on the contact surface for the different simulation cases depicted in Fig. 5 of the main text.

Figure 10 and Table 7 present the results of the EDS analyses of the tribologically transformed structure and third body layer on the surface of a steel specimen tested until failure against thin and rough HVAF coating.



**Fig. 8** Simulated contact surface pressure at the start of cyclic loading for the 250  $\mu\text{m}$  coating-to-steel contact case presented in Fig. 5 of the main text and in Fig. 9 (data common to all studied COF)



**Fig. 9** Additional simulation data for the 250  $\mu\text{m}$  coating-to-steel contact case depicted in Fig. 5 of the main text, (a) shear stress amplitude and (b) slip amplitude in the axial direction

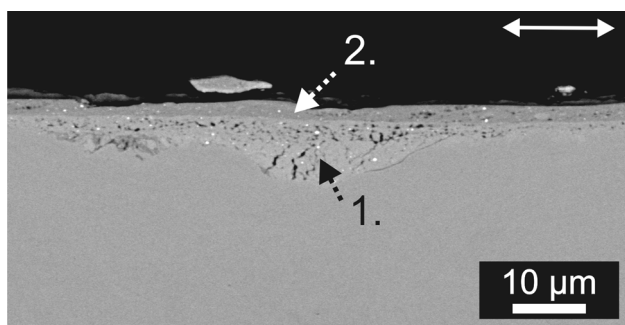


**Fig. 10** Surface of a steel specimen tested until failure against thin and rough HVOF coating. The rectangles marked with 1. and 2. denote the locations of the EDS analyses

**Acknowledgements** Dr. Juoksukangas from Tampere University is acknowledged for his help in setting up the experiments. Dr. Arto Lehtovaara, formerly a professor in Tampere University, now retired,

**Table 7** Results of the EDS analyses carried out on the locations marked in Fig. 10

Location	O	Cr	Fe	W
1.	2.3	1.5	93.7	2.5
2.	4.5	1.3	91.7	2.5

Element composition in mass-%. It should be noted that Co was not detected in the measured spectra

is acknowledged for his contributions to planning of the research, analysis of the results, and commenting the manuscript.

**Funding** Open access funding provided by Tampere University (including Tampere University Hospital). This research was funded by the Academy of Finland PerforMat project. This work made use of Tampere Microscopy Center facilities at Tampere University. Dr. Isakov acknowledges the financial support from Tampere Institute for Advanced Study.



**Data Availability** The full dataset collected during the microstructural characterization can be found in the reference Ref 53.

**Conflict of interest** On behalf of all authors, the corresponding author states that there is no conflict of interest.

**Open Access** This article is licensed under a Creative Commons Attribution 4.0 International License, which permits use, sharing, adaptation, distribution and reproduction in any medium or format, as long as you give appropriate credit to the original author(s) and the source, provide a link to the Creative Commons licence, and indicate if changes were made. The images or other third party material in this article are included in the article's Creative Commons licence, unless indicated otherwise in a credit line to the material. If material is not included in the article's Creative Commons licence and your intended use is not permitted by statutory regulation or exceeds the permitted use, you will need to obtain permission directly from the copyright holder. To view a copy of this licence, visit <http://creativecommons.org/licenses/by/4.0/>.

## References

1. A.R. Govande, A. Chandak, B.R. Sunil, and R. Dumpala, Carbide-Based Thermal Spray Coatings: A Review on Performance Characteristics and Post-Treatment, *Int. J. Refract Metal Hard Mater.*, 2022, **103**, p 105772. <https://doi.org/10.1016/j.ijrmhm.2021.105772>
2. G. Bolelli, L.-M. Berger, T. Börner, H. Koivuluoto, L. Lusvarghi, C. Lyphout, N. Markocsan, V. Matikainen, P. Nylén, P. Sassatelli, R. Trache, and P. Vuoristo, Tribology of HVOF- and HVOF-Sprayed WC-10Co4Cr Hardmetal Coatings: A Comparative Assessment, *Surf. Coat. Technol.*, 2015, **265**, p 125–144. <https://doi.org/10.1016/j.surfcoat.2015.01.048>
3. V. Eronen, S. Ahmaniemi, K. Niemi, and P. Vuoristo, Microwear in thermally sprayed hard coatings by different abrasives, in *Proceedings of the ITSC2005*. Thermal Spray 2005, in *Proceedings from the International Thermal Spray Conference*, ASM, Basel, (2005), pp. 815–822. <https://doi.org/10.31399/asm.cp.itsc2005p0815>
4. J. Kiilakoski, V. Eronen, and P. Vuoristo, Wear Properties of Thermally Sprayed Tungsten-Carbide Coatings in Paper Machine Environments, *Finn. J. Tribol.*, 2015, **33**, p 29–35.
5. A. Agüero, F. Camón, J. García de Blas, J.C. del Hoyo, R. Muelas, A. Santaballa, S. Ulargui, and P. Vallés, HVOF-Deposited WCCoCr as Replacement for Hard Cr in Landing Gear Actuators, *J. Therm. Spray Technol.*, 2011, **20**, p 1292–1309. <https://doi.org/10.1007/s11666-011-9686-1>
6. G. Matthäus, J. Henry, D. Ackermann, and W. Brandl, Further Developments in Internal Diameter HVOF Application of WC-CoCr for Hard Chrome Replacement in Critical Applications Such as Landing Gear, in *Proceedings of the ITSC2009*. Thermal Spray 2009, in *Proceedings from the International Thermal Spray Conference*, ASM, Las Vegas, Nevada, (2009) pp. 722–724. <https://doi.org/10.31399/asm.cp.itsc2009p0722>
7. R. de Medeiros Castro, A. de Silva Rocha, E. Isaías Mercado Curi, and F. Peruch, A Comparison of Microstructural, Mechanical and Tribological Properties of WC-10Co4Cr-HVOF Coating and Hard Chrome to Use in Hydraulic Cylinders, *Am. J. Mater. Sci.*, 2018, **8**, p 15–26. <https://doi.org/10.5923/j.materials.20180801.03>
8. J. Pulsford, F. Venturi, Z. Pala, S. Kamnis, and T. Hussain, Application of HVOF WC-Co-Cr Coatings on the Internal Surface of Small Cylinders: Effect of Internal Diameter on the Wear Resistance, *Wear*, 2019, **432–433**, p 202965. <https://doi.org/10.1016/j.wear.2019.202965>
9. K. Bobzin, W. Wietheger, H. Heinemann, M. Schulz, M. Oech-sner, T. Engler, H. Scheerer, and Y. Joung, Thermally Sprayed Coatings for the Valve Industry, *Materialwissenschaft und Werkstofftechnik*, 2021, **52**, p 997–1011. <https://doi.org/10.1002/mawe.202100032>
10. B.S. Mann and V. Arya, Abrasive and Erosive Wear Characteristics of Plasma Nitriding and HVOF Coatings: Their Application in Hydro Turbines, *Wear*, 2001, **249**, p 354–360. [https://doi.org/10.1016/S0043-1648\(01\)00537-3](https://doi.org/10.1016/S0043-1648(01)00537-3)
11. P. Vuoristo, Thermal Spray Coating Processes, *Comprehensive Materials Processing Coatings and films*, 1st ed., D. Cameron Ed., Elsevier, 2014, p 229–276
12. J. Juoksukangas, A. Lehtovaara, and A. Mäntylä, Experimental and Numerical Investigation of Fretting Fatigue Behavior in Bolted Joints, *Tribol. Int.*, 2016, **103**, p 440–448. <https://doi.org/10.1016/j.triboint.2016.07.021>
13. R.B. Waterhouse, *Fretting Fatigue*, Applied Science Publishers, London, 1981.
14. D.A. Hills and D. Nowell, *Mechanics of Fretting Fatigue*, Springer, 1994.
15. S. Fouvry, V. Fridrici, C. Langlade, P. Kapsa, and L. Vincent, Palliatives in Fretting: A Dynamical Approach, *Tribol. Int.*, 2006, **39**, p 1005–1015. <https://doi.org/10.1016/j.triboint.2006.02.038>
16. Y. Fu, J. Wei, and A.W. Batchelor, Some Considerations on the Mitigation of Fretting Damage by the Application of Surface-Modification Technologies, *J. Mater. Process. Technol.*, 2000, **99**, p 231–245. [https://doi.org/10.1016/S0924-0136\(99\)00429-X](https://doi.org/10.1016/S0924-0136(99)00429-X)
17. I.P. Okokpujie, L.K. Tartibu, H.O. Musa-Basheer, and A.O.M. Adeoye, Effect of Coatings on Mechanical Corrosion and Tribological Properties of Industrial Materials: A Comprehensive Review, *J. Bio-Tribo-Corros.*, 2024, **10**, p 2. <https://doi.org/10.1007/s40735-023-00805-1>
18. G. Bolelli, L.M. Berger, M. Bonetti, and L. Lusvarghi, Comparative Study of the Dry Sliding Wear Behaviour of HVOF-Sprayed WC-(W, Cr)2C-Ni and WC-CoCr Hardmetal Coatings, *Wear*, 2014, **309**, p 96–111. <https://doi.org/10.1016/j.wear.2013.11.001>
19. J.K.N. Murthy and B. Venkataraman, Abrasive Wear Behaviour of WC-CoCr and Cr<sub>3</sub>C<sub>2</sub>-20(NiCr) Deposited by HVOF and Detonation Spray Processes, *Surf. Coat. Technol.*, 2006, **200**, p 2642–2652. <https://doi.org/10.1016/j.surfcoat.2004.10.136>
20. Q. Wang, S. Zhang, Y. Cheng, J. Xiang, X. Zhao, and G. Yang, Wear and Corrosion Performance of WC-10Co4Cr Coatings Deposited by Different HVOF and HVOF Spraying Processes, *Surf. Coat. Technol.*, 2013, **218**, p 127–136. <https://doi.org/10.1016/j.surfcoat.2012.12.041>
21. A.C. Karaoglanli, M. Oge, K.M. Doleker, and M. Hotamis, Comparison of Tribological Properties of HVOF Sprayed Coatings with Different Composition, *Surf. Coat. Technol.*, 2017, **318**, p 299–308. <https://doi.org/10.1016/j.surfcoat.2017.02.021>
22. T. Varis, T. Suhonen, J. Laakso, M. Jokipii, and P. Vuoristo, Evaluation of Residual Stresses and Their Influence on Cavitation Erosion Resistance of High Kinetic HVOF and HVOF-Sprayed WC-CoCr Coatings, *J. Therm. Spray Technol.*, 2020, **29**, p 1365–1381. <https://doi.org/10.1007/s11666-020-01037-2>
23. V. Matikainen, H. Koivuluoto, P. Vuoristo, J. Schubert, and Š Houdková, Effect of Nozzle Geometry on the Microstructure and Properties of HVOF-Sprayed WC-10Co4Cr and Cr3C2-25NiCr Coatings, *J. Therm. Spray Technol.*, 2018, **27**, p 680–694. <https://doi.org/10.1007/s11666-018-0717-z>
24. V. Matikainen, S. Rubio Peregrina, N. Ojala, H. Koivuluoto, J. Schubert, Š Houdková, and P. Vuoristo, Erosion Wear Performance of WC-10Co4Cr and Cr3C2-25NiCr Coatings Sprayed with High-Velocity Thermal Spray Processes, *Surf. Coat.*

- Technol.*, 2019, **370**, p 196–212. <https://doi.org/10.1016/j.surfcoat.2019.04.067>
25. A. Vackel and S. Sampath, Fatigue Behavior of Thermal Sprayed WC-CoCr- Steel Systems: Role of Process and Deposition Parameters, *Surf. Coat. Technol.*, 2017, **315**, p 408–416. <https://doi.org/10.1016/j.surfcoat.2017.02.062>
  26. R.T.R. McGrann, D.J. Greving, J.R. Shadley, E.F. Rybicki, T.L. Kruecke, and B.E. Bodger, The Effect of Coating Residual Stress on the Fatigue Life of Thermal Spray-Coated Steel and Aluminum, *Surf. Coat. Technol.*, 1998, **108–109**, p 59–64. [https://doi.org/10.1016/S0257-8972\(98\)00665-3](https://doi.org/10.1016/S0257-8972(98)00665-3)
  27. H.J.C. Voorwald, R.C. Souza, W.L. Pigatin, and M.O.H. Cioffi, Evaluation of WC-17Co and WC-10Co-4Cr Thermal Spray Coatings by HVOF on the Fatigue and Corrosion Strength of AISI 4340 Steel, *Surf. Coat. Technol.*, 2005, **190**, p 155–164. <https://doi.org/10.1016/j.surfcoat.2004.08.181>
  28. J.G. La Barbera-Sosa, Y.Y. Santana, C. Villalobos-Gutiérrez, D. Chicot, J. Lesage, X. Decoopman, A. Iost, M.H. Staia, and E.S. Puchi-Cabrera, Fatigue Behavior of a Structural Steel Coated with a WC-10Co-4Cr/Colmonoy 88 Deposit by HVOF Thermal Spraying, *Surf. Coat. Technol.*, 2013, **220**, p 248–256. <https://doi.org/10.1016/j.surfcoat.2012.05.098>
  29. D. Du, D. Liu, X. Zhang, J. Tang, and B. Meng, Effects of WC-17Co Coating Combined with Shot Peening Treatment on Fatigue Behaviors of TC21 Titanium Alloy, *Materials*, 2016, **9**, p 865. <https://doi.org/10.3390/ma9110865>
  30. C.H. Sathisha, B.N. Ravikumar, K. Anand, and T. Shalini, Elevated Temperature Fretting Wear Behavior of Cobalt-Based Alloys, *J. Tribol.*, 2016, **138**, p 031601. <https://doi.org/10.1115/1.4031831>
  31. G. Lv, X. Yang, T. Gao, S. Wang, J. Xiao, Y. Zhang, K. Chen, and H. Yang, Investigation on Fretting Wear Performance of Laser Cladding WC/Co6 Coating on 42CrMo Steel for Hydraulic Damper, *Int. J. Refract Metal Hard Mater.*, 2023, **111**, p 106068. <https://doi.org/10.1016/j.ijrmhm.2022.106068>
  32. K. Kubiak, S. Fouvry, and A.M. Marechal, A Practical Methodology to Select Fretting Palliatives: Application to Shot Peening, Hard Chromium and WC-Co Coatings, *Wear*, 2005, **259**, p 367–376. <https://doi.org/10.1016/j.wear.2005.01.030>
  33. K. Kubiak, S. Fouvry, A.M. Marechal, and J.M. Vernet, Behaviour of Shot Peening Combined with WC-Co HVOF Coating under Complex Fretting Wear and Fretting Fatigue Loading Conditions, *Surf. Coat. Technol.*, 2006, **201**, p 4323–4328. <https://doi.org/10.1016/j.surfcoat.2006.08.094>
  34. M. Okane, K. Shiozawa, M. Hiki, and K. Suzuki, Fretting Fatigue Properties of WC-Co Thermal Sprayed NiCrMo Steel, Fretting Fatigue, *Advances in the Basic Understanding and Applications ASTM STP 1425*. Y. Mutoh, S.E. Kinyon, D.W. Hoepfner Ed., ASTM International, West Conshohocken, 2003, p 385–399
  35. X.X. Wang, X.C. Ping, X. Zeng, R.J. Wang, Q. Zhao, S.J. Ying, and T. Hu, Fretting Fatigue Experiment and Simulation of WC-12Co Coating Taking into Account the Wear Effects, *Surf. Coat. Technol.*, 2022, **441**, p 128555. <https://doi.org/10.1016/j.surfcoat.2022.128555>
  36. X. Zeng, X. Wang, X. Ping, R. Wang, and T. Hu, Research on Fretting Fatigue of Tungsten Carbide Coating Based on Strain Energy Density Methods, *Arch. Metall. Mater.*, 2023, **68**(1), p 21–30. <https://doi.org/10.24425/amm.2023.141467>
  37. J. Hintikka, A. Lehtovaara, and A. Mäntylä, Fretting-Induced Friction and Wear in Large Flat-on-Flat Contact with Quenched and Tempered Steel, *Tribol. Int.*, 2015, **92**, p 191–202. <https://doi.org/10.1016/j.triboint.2015.06.008>
  38. Y.C. Tsui and T.W. Clyne, An Analytical Model for Predicting Residual Stresses in Progressively Deposited Coatings: Part 1: Planar Geometry, *Thin Solid Films*, 1997, **306**, p 23–33. [https://doi.org/10.1016/S0040-6090\(97\)00199-5](https://doi.org/10.1016/S0040-6090(97)00199-5)
  39. T. Suhonen, T. Varis, E. Turunen, X. Liu, Y. Ge, O. Söderberg, and S.-P. Hannula, The Effect of Microstructure on Mechanical Properties of HVOF Sprayed WC-CoCr Composite Coatings, *Tribology*, 2009, **28**, p 14–28.
  40. Y.C. Tsui, and T.W. Clyne, An Analytical Model for Predicting Residual Stresses in Progressively Deposited Coatings: Part 3: Further Development and Applications, *Thin Solid Films*, 1997, **306**, p 52–61. [https://doi.org/10.1016/S0040-6090\(97\)00208-3](https://doi.org/10.1016/S0040-6090(97)00208-3)
  41. J. Matejcek, S. Sampath, D. Gilmore, and R. Neiser, In Situ Measurement of Residual Stresses and Elastic Moduli in Thermal Sprayed Coatings Part 2: Processing Effects on Properties of Mo Coatings, *Acta Mater.*, 2003, **51**, p 873–885. [https://doi.org/10.1016/S1359-6454\(02\)00477-9](https://doi.org/10.1016/S1359-6454(02)00477-9)
  42. T. Varis, T. Suhonen, M. Jokipii, and P. Vuoristo, Influence of Powder Properties on Residual Stresses Formed in High-Pressure Liquid Fuel HVOF Sprayed WC-CoCr Coatings, *Surf. Coat. Technol.*, 2020, **388**, p 125604. <https://doi.org/10.1016/j.surfcoat.2020.125604>
  43. K. Fan, W. Jiang, V. Luzin, T. Gong, W. Feng, J. Ruiz-Hervias, and P. Yao, Influence of WC Particle Size on the Mechanical Properties and Residual Stress of HVOF Thermally Sprayed WC-10Co-4Cr Coatings, *Materials*, 2022, **15**, p 5537. <https://doi.org/10.3390/ma15165537>
  44. L. Rajanna, T.G. Mamatha, M.S. Prabhswamy, V. Singh, and A. Bansal, Performance of HVOF Sprayed WC-10Co-4Cr Coating Onto Cast 21–4N Steel for Slurry Erosion: Characterization and Erosion Rate Studies, *Proc. Inst. Mech. Eng. Part C J. Mech. Eng. Sci.*, 2023 <https://doi.org/10.1177/09544062231211717>
  45. E. Leidich, A. Maiwald, and J. Vidner, A Proposal for a Fretting Wear Criterion for Coated Systems with Complete Contact Based on Accumulated Friction Energy Density, *Wear*, 2013, **297**, p 903–910. <https://doi.org/10.1016/j.wear.2012.11.006>
  46. V. Nurmi, J. Hintikka, J. Juoksukangas, M. Honkanen, M. Vippola, A. Lehtovaara, A. Mäntylä, J. Vaara, and T. Frondelius, The Formation and Characterization of Fretting-Induced Degradation Layers Using Quenched and Tempered Steel, *Tribol. Int.*, 2019, **131**, p 258–267. <https://doi.org/10.1016/j.triboint.2018.09.012>
  47. B.D. Leonard, A. Ghosh, F. Sadeghi, S. Shinde, and M. Mittelbach, Third Body Modeling in Fretting Using the Combined Finite-Discrete Element Method, *Int. J. Solids Struct.*, 2014, **51**, p 1375–1389. <https://doi.org/10.1016/j.ijsostr.2013.12.036>
  48. A.M. Kirk, P.H. Shipway, W. Sun, and C.J. Bennett, The Effect of Frequency on Both the Debris and the Development of the Tribologically Transformed Structure During Fretting Wear of a High Strength Steel, *Wear*, 2019, **426–427**, p 694–703. <https://doi.org/10.1016/j.wear.2018.12.035>
  49. J. Hintikka, A. Lehtovaara, and A. Mäntylä, Third Particle Ejection Effects on Wear with Quenched and Tempered Steel Fretting Contact, *Tribol. Trans.*, 2017, **60**, p 70–78. <https://doi.org/10.1080/10402004.2016.1146813>
  50. C. Colombie, Y. Berthier, A. Floquet, L. Vincent, and M. Godet, Fretting: Load Carrying Capacity of Wear Debris, *J. Tribol.*, 1984, **106**, p 194–201. <https://doi.org/10.1115/1.3260881>
  51. M. Gui, R. Eybel, B. Asselin, and F. Monerie-Moulin, Cracking and Spalling Behavior of HVOF Thermally Sprayed WC-Co-Cr Coating in Bend and Axial Fatigue Tests, *J. Mater. Eng. Perform.*, 2015, **24**, p 1347–1356. <https://doi.org/10.1007/s11665-014-1378-9>
  52. G.W. Schulze and F. Erdogan, Periodic Cracking of Elastic Coatings, *Int. J. Solids Struct.*, 1998, **35**, p 3615–3634. [https://doi.org/10.1016/S0020-7683\(97\)00228-X](https://doi.org/10.1016/S0020-7683(97)00228-X)
  53. V. Haaja, T. Varis, J. Laurila, and M. Isakov, PerforMat Project, Use Case 1, Microstructural Characterisation Data, IDA FAIR-DATA, (2023). <https://doi.org/10.23729/94675246-8435-436d-a872-110cb8ca699d>

**Publisher's Note** Springer Nature remains neutral with regard to jurisdictional claims in published maps and institutional affiliations.